Mechanical Systems and Signal Processing 122 (2019) 658–672

Contents lists available at ScienceDirect

Mechanical Systems and Signal Processing

journal homepage: www.elsevier.com/locate/ymssp

Nested adaptive super-twisting sliding mode control design for a vehicle steer-by-wire system

Zhe Sun [a,*], Jinchuan Zheng [a], Zhihong Man [a], Minyue Fu [b], Renquan Lu [c]

[a] Faculty of Science, Engineering and Technology, Swinburne University of Technology, John St, Hawthorn, VIC 3122, Australia
[b] School of Electrical Engineering and Computer Science, University of Newcastle, Callaghan, NSW 2308, Australia
[c] School of Automation and Guangdong Key Laboratory of IoT Information Technology, Guangdong University of Technology, Guangzhou 510006, China

ARTICLE INFO

Article history:
Received 4 August 2018
Received in revised form 20 December 2018
Accepted 22 December 2018

Keywords:
Adaptive control
Super-twisting sliding mode
Steer-by-wire
Self-aligning torque

ABSTRACT

This paper presents a nested adaptive super-twisting sliding mode (NASTSM) control scheme for a vehicle Steer-by-Wire (SbW) system. Firstly, the plant model of the SbW system is expressed as a second-order differential equation from the steering motor input voltage to the front wheel steering angle. Specifically, the model of the self-aligning torque is elaborated in detail and compared with a simplified one. Next, an NASTSM controller is designed for the SbW system, which adopts a nested adaptive law to promote tracking accuracy by dealing with complex time-varying external disturbances and a super-twisting sliding mode (STSM) control component to guarantee strong robustness while alleviating chattering phenomenon. The stability of the NASTSM control system is verified in the sense of Lyapunov. Finally, experiments are carried out under various conditions. The experimental results show that the proposed NASTSM controller owns superiority in terms of not only higher tracking precision and stronger robustness, but also less dependence on the information of plant models compared with a conventional adaptive sliding mode (CASM) controller.

1. Introduction

As a new trend in the development of automobile industry, the by-wire technology has been investigated and implemented in almost every part of modern vehicles, such as steer-by-wire (SbW) [1,2], brake-by-wire [3,4], throttle-by-wire [5], shift-by-wire [6] and accelerate-by-wire [7]. As a pivotal part of vehicle by-wire technologies, an SbW system uses a steering motor to generate torques for steering front wheels, a feedback motor to generate feedback torques for drivers to perceive the interactions between front wheels and road surfaces, and an electronic control system to control the whole SbW system [8]. The SbW technology possesses noteworthy advantages in comparison with traditional steering systems, such as the enhancement of a vehicle's mobility and maneuverability while guaranteeing high-fidelity steering feel [9] and the reduction of noises, vibrations, environmental concerns and energy consumptions of a vehicle [10]. In addition, the SbW technology is an important foundation of self-driving automobiles which are the future of transportation [7].

For the aim of forcing an SbW equipped vehicle to follow a road path fast and precisely, accurate dynamic modeling and robust control design are both crucial. Dynamic models of SbW systems are investigated by many researchers. For instance, a

* Corresponding author.
E-mail addresses: zsun@swin.edu.au (Z. Sun), jzheng@swin.edu.au (J. Zheng), zman@swin.edu.au (Z. Man), minyue.fu@newcastle.edu.au (M. Fu), rqlu@gdut.edu.cn (R. Lu).

https://doi.org/10.1016/j.ymssp.2018.12.050
0888-3270/

bicycle model with detailed description of self-aligning torques is proposed to elaborate a vehicle's dynamics in the horizontal plane [11]. In [12], a plant model of an SbW system including the bound information of system parameters, a simplified model of self-aligning torques and a model from the d-q-axis stator voltages to output torques of a steering motor is described in detail. Apart from modeling, robust control design for SbW systems is also of great importance. A number of control schemes have been proposed for vehicle steering systems, such as sliding mode-based control [13,14], fuzzy scheduled optimal control [15] and neural network control [16]. In [17], a model predictive controller is designed for a vehicle SbW system, which owns fault-tolerant property.

As a variable structure control method, sliding mode control uses a switching control signal to force the system to 'slide' along a sliding surface, which performs strong robustness against system uncertainties and disturbances [18]. Due to its merits, sliding mode control has been used in many applications, such as [19–22]. On the basis of conventional sliding mode control, a terminal sliding mode (TSM) control method is proposed to increase the convergence rate and alleviate the chattering phenomenon [23]. Afterwards, non-singular terminal sliding mode (NTSM) control is presented to settle the singularity problem existing in TSM control [24]. Furthermore, super-twisting sliding mode (STSM) control is proposed, which can generate continuous control signals, handle system uncertainties and attain finite-time convergence property [25]. For instance, an STSM control scheme is proposed for a breathing subsystem of a polymer electrolyte membrane fuel cell stack, which demonstrates distinctive robust features and control smoothness [26]. Adaptive control is another powerful control method specifically effective for systems with time-varying parameters or dynamics [27–29]. For instance, a novel adaptive robust triple-step control scheme is proposed to compensate for cogging torques in a dc motor, where an adaptive algorithm is employed to identify unknown parameters online and a model-based triple-step nonlinear control component is presented to deal with system uncertainties and achieve robust control performance [30]. Recently, Edwards et. al. have presented a novel nested adaptive control method which demonstrates good control performance without the bound information of adaptation gains, external disturbances and their derivatives [31]. The nested adaptive control and the STSM control have their own advantages, but the combination of them is still rare in actual implementations, especially in SbW systems. Thus, it motivates us to combine them and design a nested adaptive super-twisting sliding mode (NASTSM) controller for vehicle SbW systems.

In this paper, an NASTSM control scheme is proposed for a vehicle SbW system. In the NASTSM control, a nested adaptive law is adopted to cope with complex time-varying external disturbances but requiring less model information compared with ordinary adaptive laws, and an STSM control component is designed to maintain finite-time convergence and chattering-alleviation. Superior control performance is obtained for the NASTSM controller in comparison with a conventional adaptive sliding mode (CASM) controller proposed in [13].

The remaining part is organized as follows. In Section 2, the dynamic model of the SbW system is described in detail, especially the model of self-aligning torques. In Section 3, the NASTSM controller is designed for the SbW system, and the stability of the whole system is proved in the sense of Lyapunov. In Section 4, experimental results of the NASTSM and CASM controllers are shown, compared and analyzed. Finally, Section 5 concludes this paper.

2. Plant modeling

Our experimental platform of a vehicle SbW system is shown in Fig. 1, where the conventional steering column between the steering wheel and the pinion-and-rack system is removed and replaced by a steering motor (Mitsubishi HF-SP102). The steering motor is controlled to provide appropriate torques to steer the front wheels through a gear head, a pinion-and-rack gear box and steering arms. Designed controllers are executed by using MATLAB Real-Time Workshops installed in an HP computer. An Advantech PCI multifunction card is used to collect sensor measurements and generate control inputs in real time. A servo driver is used to convert the control input signals to current signals to drive the steering motor. An angle sensor (MoTeC) is installed on the pinion to measure the rotary angle of the pinion. Multiplying this angle measurement by a transmission gain from the pinion to the front wheels yields the steering angle of the front wheels, i.e., the system output to be controlled. As shown in Fig. 1(b), another angle sensor (MoTeC) is installed on the column of the steering wheel to measure the rotary angle of the steering wheel manipulated by a driver. Likewise, multiplying this angle measurement by a transmission gain from the steering wheel to the front wheels yields the reference command of the closed-loop control system.

According to a bicycle model proposed in [11], the plant model of our SbW system can be expressed by

$$\begin{aligned} J\ddot{\delta} + c\dot{\delta} &= bu - F - \tau \\ F &= f\,\mathrm{sign}(\dot{\delta}) \end{aligned} \tag{1}$$

where J and c denote the equivalent moment of inertia and the viscous friction of the steering system, respectively; δ is the steering angle of the front wheels, i.e., the system output; F is the Coulomb friction with a coefficient of f and a standard signum function $\mathrm{sign}(\dot{\delta})$; τ represents the self-aligning torque acting on the front wheels; u is the control input of the closed-loop control system; b is a gain consisting of four components, i.e., the scale factor accounting for the conversion from input voltages to output torques of the steering motor, the gear ratio of the gear head, the gear ratio of the pinion-and-rack system and the transmission gain from the linear motion of the rack to the steering motion of the front wheels. Due to a high bandwidth of the steering motor and the mechanical property of our experimental platform, the variation of the value of b is almost negligible. Thus, b is treated as a constant with the value of

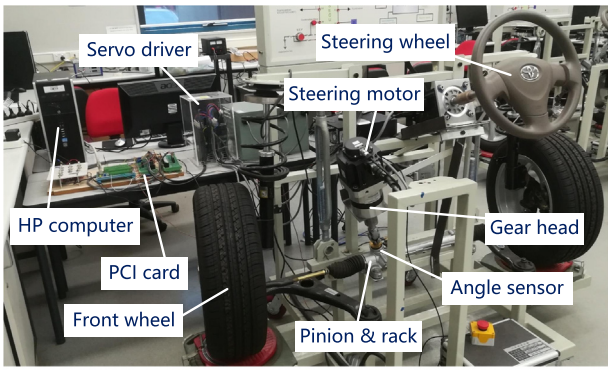

(a)

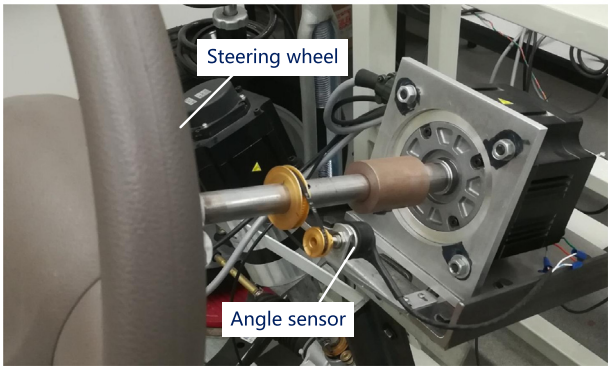

(b)

Fig. 1. Experimental platform of an SbW system.

$$b = 275 \text{ Nm/V}. \tag{2}$$

Note that there exist parametric uncertainties in the system. Thus, we can rewrite (1) as

$$J_0\ddot{\delta} + c_0\dot{\delta} + f_0\text{sign}(\dot{\delta}) + \tau_0 + \Delta = bu \tag{3}$$

where J_0, c_0, f_0 and τ_0 denote the nominal parameters of J, c, f and τ, respectively; Δ represents the lumped uncertainties existing in the system. The nominal values of the parameters are known as

$$\begin{aligned} J_0 &= 60 \text{ kgm}^2 \\ c_0 &= 152 \text{ Nms/rad} \\ f_0 &= 5 \text{ Nm}. \end{aligned} \tag{4}$$

And the lumped uncertainties Δ satisfies

$$|\Delta| \leqslant \bar{\Delta} = 100 \text{ Nm} \tag{5}$$

where $\bar{\Delta}$ is the upper bound of Δ.

Note that the proposed NASTSM control does not require the bound information of each parameter. However, the CASM control presented for comparison requires the bound information of all parameters. Thus, we give this information here:

$$\begin{aligned} |\Delta_J| &= |J - J_0| \leqslant \bar{\Delta}_J = 6 \text{ kgm}^2 \\ |\Delta_c| &= |c - c_0| \leqslant \bar{\Delta}_c = 15 \text{ Nms/rad} \\ |\Delta_f| &= |f - f_0| \leqslant \bar{\Delta}_f = 0.5 \text{ Nm} \end{aligned} \tag{6}$$

where Δ_J, Δ_c and Δ_f are the corresponding parametric uncertainties of J, c and f; $\bar{\Delta}_J, \bar{\Delta}_c$ and $\bar{\Delta}_f$ are the upper bounds of Δ_J, Δ_c and Δ_f, respectively.

Fig. 2 shows the generation of self-aligning torques acting on the front wheel [11]. Related parameters with values are given in Tables 1 and 2 [11,12]. Specifically, the pneumatic trail t_p means the distance between the center of the wheel

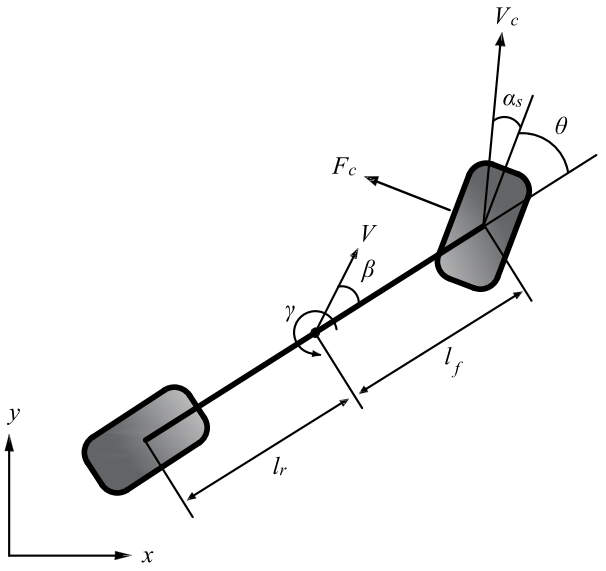

(a) A simplified bicycle model for vehicles

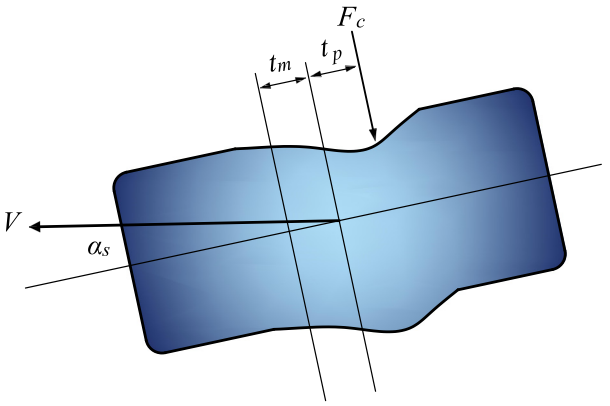

(b) Front tire operating under a lateral force

Fig. 2. Modeling of self-aligning torque.

Table 1
Parameters of self-aligning torque model.

Parameter	Description
δ	Front wheel steering angle
F_c	Front wheel lateral force
α_s	Front wheel slip angle
V	Vehicle velocity at center of gravity (CG)
V_c	Velocity of front wheel
β	Vehicle body slip angle at CG
γ	Vehicle yaw rate
l_f	Distance between the center of front wheel and CG
l_r	Distance between the center of rear wheel and CG
C_f	Front wheel cornering stiffness
C_r	Rear wheel cornering stiffness
t_m	Front wheel mechanical trail
t_p	Front wheel pneumatic trail
m	Vehicle mass
I_z	Vehicle inertia around CG

Table 2
Values of Vehicle Parameters.

Parameter	Value
t_m, t_p	0.015 m, 0.023 m
l_f, l_r	1.2 m, 1.05 m
m	2000 kg
C_f, C_r for wet asphalt road	45,000 N/rad
C_f, C_r for dry asphalt road	80,000 N/rad
C_f, C_r for snowy road	12,000 N/rad

and the application point of the lateral force; the mechanical trail t_m means the distance between the center of the wheel and the point on road surfaces where the wheel pivots. Then, the self-aligning torque can be expressed as

$$\tau_0 = F_c \cdot (t_m + t_p). \tag{7}$$

Under the condition of a small slip angle α_s, the lateral force F_c has a linear relationship with α_s:

$$F_c = -C_f \cdot \alpha_s \tag{8}$$

where C_f is the cornering stiffness of the front wheel, and α_s is given by [32]

$$\alpha_s = \beta + \frac{\gamma l_f}{V} - \delta. \tag{9}$$

Hence, substituting (9) into (8) yields the lateral force F_c as

$$F_c = -C_f\left(\beta + \frac{\gamma l_f}{V} - \delta\right). \tag{10}$$

Combining (7) with (10), the self-aligning torque τ_0 can be expressed as

$$\tau_0 = -C_f(t_m + t_p)\left(\beta + \frac{\gamma l_f}{V} - \delta\right). \tag{11}$$

Actually, the slip angle of the vehicle β can be obtained from the following expression:

$$\beta = \tan^{-1}\left[\frac{l_r}{l_f + l_r} \cdot \tan(\delta)\right]. \tag{12}$$

Furthermore, the yaw motion of the vehicle can be described by a state-space equation [12] shown as follows:

$$\begin{bmatrix} \dot{\beta} \\ \dot{\gamma} \end{bmatrix} = \begin{bmatrix} \frac{-C_f - C_r}{mV} & -1 + \frac{C_r l_r - C_f l_f}{mV^2} \\ \frac{C_r l_r - C_f l_f}{I_z} & \frac{-C_f l_f^2 - C_r l_r^2}{I_z V} \end{bmatrix} \cdot \begin{bmatrix} \beta \\ \gamma \end{bmatrix} + \begin{bmatrix} \frac{C_f}{mV} \\ \frac{C_f l_f}{I_z} \end{bmatrix} \delta. \tag{13}$$

Rearranging (13) yields the vehicle yaw rate γ as

$$\gamma = \left(\dot{\beta} + \frac{C_f + C_r}{mV}\beta - \frac{C_f}{mV}\delta\right) \cdot \left(\frac{C_r l_r - C_f l_f}{mV^2} - 1\right)^{-1}. \tag{14}$$

Therefore, the complete model of the self-aligning torque τ_0 can be obtained by combining (11), (12) and (14).

In our case, the values of the parameters in the self-aligning torque model are listed in Table 2 [12]. Under the condition of a constant vehicle velocity V, a hyperbolic tangent signal is used to mimic the self-aligning torque in [13], which is expressed as

$$\tau_0 = \rho_\tau \cdot \tanh(\delta) \tag{15}$$

where ρ_τ is a time-varying coefficient with respect to road conditions, and $\tanh(*)$ denotes the hyperbolic tangent function

$$\tanh(x) = \frac{e^{2x} - 1}{e^{2x} + 1}. \tag{16}$$

Under the condition of $V = 35$ m/s, the values of ρ_τ can be given by

$$\rho_\tau = \begin{cases} 250, & \text{snowy road} \\ 950, & \text{wet asphalt road} \\ 1760, & \text{dry asphalt road} \end{cases} \tag{17}$$

to mimic the self-aligning torques under the conditions of a snowy road, a wet asphalt road and a dry asphalt road, respectively.

According to the complete model of the self-aligning torque given by (8)–(14) and the simplified model shown in (15), the actual self-aligning torque and the simplified one under the condition of snowy road are plotted in Fig. 3. In Fig. 3(a), the vehicle velocity is set as $V = 35$ m/s, and the values of vehicle parameters are set as the nominal ones listed in Table 2. We can see that under this condition the simplified self-aligning torque conforms to the actual one pretty well. However, if we set $m = 2400$ kg, $V = 15$ m/s and add some uncertainties to C_f and C_r, the simplified self-aligning torque cannot conform to the actual one satisfactorily as shown in Fig. 3(b). Thus, the simplified model given by (15) has limitations and cannot describe the actual self-aligning torque well enough under a wider range of vehicle conditions. This implies that the model-based CASM controller proposed in [13] may have performance limitation in practice. Therefore, this motivates us to investigate a new control method in this paper which does not rely on the self-aligning torque model. For comparison in experiments, we will set the vehicle velocity V with a time-varying value, which is closer to the reality and can demonstrate the strong robustness of the proposed control scheme against the variation of V.

Limited by our experimental platform, the front wheels shown in Fig. 1 cannot be driven to generate forward velocity. Thus, the ground cannot generate real self-aligning torque and exert it on the front wheels during the experiment. However, the other dynamics of our SbW system are real and can be directly validated in experiments. Since the detailed and accurate model of the self-aligning torques has been given by (11), (12) and (14) with the values of all the related parameters shown in Table 2, we can artificially generate the following voltage signal as an input to the steering motor:

$$u_\tau = \frac{\tau_0}{b} + n_w \tag{18}$$

where τ_0 is given by (11), and n_w is a white noise signal added to simulate the parametric uncertainties existing in the self-aligning torque model since all the values of the parameters given by Table 2 are nominal ones. Then, after the conversion from input voltages to output torques through the steering motor, the amplification through the gear head, and the transmission through the pinion-and-rack system and the steering arms as shown in Fig. 1, the effect of the self-aligning torques can be generated and exerted on the front wheels. Note that u_τ defined in (18) is thoroughly independent from the control input u mentioned in (1). Thus, we can reasonably treat the effect of the self-aligning torques generated by u_τ as an external disturbance of the whole system. The purpose of elaborating the actual self-aligning torque model is to obtain the voltage signal given by (18) in experiments. However, we should note that the designed NASTSM controller is almost a model-free controller that does not require the information of the self-aligning torque model, which is a prominent benefit compared with other model-dependent controllers.

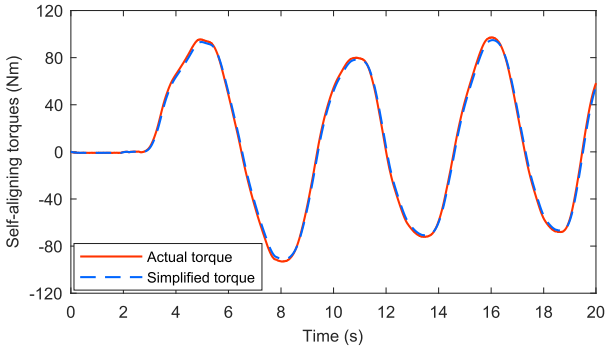

(a) Model under nominal conditions

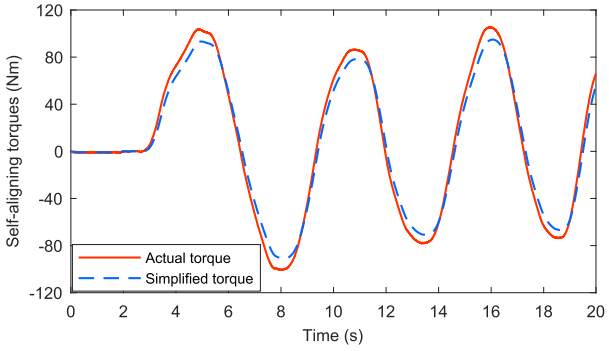

(b) Mismatched under varying conditions

Fig. 3. Simulation of self-aligning torque model.

3. Control design

Our aim is to design a robust controller which can force the front wheel steering angle to track the reference command fast and precisely under parametric uncertainties and unmodeled dynamics. Besides, due to the complex model of the self-aligning torque, we expect that the designed controller does not require the bound information of the external disturbances in the system. Thus, an NASTSM control scheme is proposed for the SbW system. In the NASTSM control, the nested adaptive law can handle the complex time-varying self-aligning torque and the STSM control component can smooth the control signal while guaranteeing strong robustness and fast time-convergence property.

3.1. NASTSM control design for SbW systems

Considering the plant model given by (1), we design the control input u as

$$u = \frac{J_0}{b}\left[\frac{f_0 \mathrm{sign}(\dot{\delta})}{J_0} + u_c\right] \tag{19}$$

where u_c is a control input component to be designed later. Substituting (19) into (1) yields

$$\ddot{\delta} + \frac{c_0}{J_0}\dot{\delta} + \frac{\tau_0}{J_0} + \frac{\Delta}{J_0} = u_c \tag{20}$$

which can be regarded as an equivalent plant model of the SbW system. Thus, our aim is to design u_c to obtain a satisfactory control performance. Initially, we define the tracking error of the control system e as

$$e = \delta - \delta_r \tag{21}$$

where δ_r is the reference command for the front wheel steering angle to track, which is usually twice-differentiable due to common curves of roads. Afterwards, we define a sliding variable s as

$$s = \dot{e} + \lambda e \tag{22}$$

where $\lambda > 0$ is a control parameter to be designed. Then, we can get the first-order derivative of the sliding variable s as follows

$$\begin{aligned} \dot{s} &= \ddot{e} + \lambda \dot{e} \\ &= \ddot{\delta} - \ddot{\delta}_r + \lambda\dot{\delta} - \lambda\dot{\delta}_r. \end{aligned} \tag{23}$$

From (20) we get

$$\ddot{\delta} = -\frac{c_0}{J_0}\dot{\delta} - \frac{\tau_0}{J_0} - \frac{\Delta}{J_0} + u_c. \tag{24}$$

Substituting (24) into (23) yields

$$\begin{aligned} \dot{s} &= A(t) + u_c \\ A(t) &= \left(\lambda - \tfrac{c_0}{J_0}\right)\dot{\delta} - \ddot{\delta}_r - \lambda\dot{\delta}_r - \tfrac{\tau_0}{J_0} - \tfrac{\Delta}{J_0} \end{aligned} \tag{25}$$

where $A(t)$ is a continuous and twice differentiable term which is supposed to satisfy $|A(t)| \leqslant A_0, |\dot{A}(t)| \leqslant A_1$ and $|\ddot{A}(t)| \leqslant A_2$. The parameters A_0, A_1 and A_2 are unknown constants, and they denote the upper bounds of $A(t), \dot{A}(t)$ and $\ddot{A}(t)$, respectively.

Let the control input component u_c be [31]

$$\begin{aligned} u_c &= -\mu|s|^{\frac{1}{2}}\mathrm{sign}(s) + v(t) \\ \dot{v}(t) &= -h(t)\mathrm{sign}(s) \end{aligned} \tag{26}$$

where $\mu > 0$ is to be designed, and $h(t)$ contains a nested adaption law shown as follows:

$$\begin{aligned} \dot{h}(t) &= -[\rho_0 + \rho(t)]\mathrm{sign}(g(t)) \\ \dot{\rho}(t) &= \begin{cases} \omega|g(t)| & \text{if} |g(t)| > g_0 \\ 0 & \text{otherwise} \end{cases} \\ g(t) &= h(t) - \tfrac{1}{\eta}|\bar{\varphi}_{eq}(t)| - \xi \\ \varphi(t) &= h(t)\mathrm{sign}(s) \\ \dot{\bar{\varphi}}_{eq}(t) &= \tfrac{1}{\epsilon}[\varphi(t) - \bar{\varphi}_{eq}(t)] \end{cases} \end{aligned} \tag{27}$$

where $\mu > 0, \rho_0 > 0, \omega > 0, g_0 > 0, 0 < \eta < 1, \xi > 0$ and $\epsilon > 0$ are constants to be designed. For the convenience of control design, we define

$$z(t) = \frac{qA_2}{\eta} - \rho(t) \tag{28}$$

where $q > 1$ indicates the so-called safety margin [31].

Then, the design parameters are chosen to satisfy the following conditions [31]:

$$\begin{aligned} &\tfrac{1}{\eta}|\bar{\varphi}_{eq}(t)| + \tfrac{\xi}{2} > |\varphi_{eq}(t)| \\ &\tfrac{1}{4}\xi^2 > g_0^2 + \tfrac{1}{\omega}\left(\tfrac{qA_2}{\eta}\right)^2 \\ &|\dot{\bar{\varphi}}_{eq}(t)| < qA_2. \end{aligned} \tag{29}$$

Lemma 1. *Consider the SbW system (1) with the parametric uncertainties in (5) and under the NASTSM control law given by (19), (26) and (27). Then, the tracking error defined in (21) can converge to zero for a given reference angle signal.*

Proof. Since we have defined $z(t) = \frac{qA_2}{\eta} - \rho(t)$, we can get

$$\rho(t) = \frac{qA_2}{\eta} - z(t). \tag{30}$$

Then, a Lyapunov function V is defined as

$$V = \frac{1}{2}g(t)^2 + \frac{1}{2\omega}z(t)^2. \tag{31}$$

According to the expression of $g(t)$ and $h(t)$ given by (27) and the expression of $\rho(t)$ given by (30), we get the first-order derivative of $g(t)$ as

$$\begin{aligned} \dot{g}(t) = &\ \dot{h}(t) - \tfrac{1}{\eta}|\dot{\bar{\varphi}}_{eq}(t)| \\ = &\ -[\rho_0 + \rho(t)]\mathrm{sign}(g(t)) - \tfrac{1}{\eta}|\dot{\bar{\varphi}}_{eq}(t)| \\ = &\ -\left[\rho_0 + \tfrac{qA_2}{\eta} - z(t)\right]\mathrm{sign}(g(t)) - \tfrac{1}{\eta}|\dot{\bar{\varphi}}_{eq}(t)|. \end{aligned} \tag{32}$$

Based on (32) and (29), we obtain

$$\begin{aligned} g\dot{g} = &\ -\left[\rho_0 + \tfrac{qA_2}{\eta} - z(t)\right]|g| - \tfrac{g}{\eta}|\dot{\bar{\varphi}}_{eq}(t)| \\ = &\ -\rho_0|g| - \tfrac{qA_2}{\eta}|g| + z(t)|g| - \tfrac{g}{\eta}|\dot{\bar{\varphi}}_{eq}(t)| \\ \leqslant &\ -\rho_0|g| - \tfrac{qA_2}{\eta}|g| + z(t)|g| + \tfrac{|g|}{\eta}|\dot{\bar{\varphi}}_{eq}(t)| \\ \leqslant &\ -\rho_0|g| - \tfrac{qA_2}{\eta}|g| + z(t)|g| + \tfrac{qA_2}{\eta}|g| \\ = &\ -\rho_0|g| + z(t)|g|. \end{aligned} \tag{33}$$

The definition of $\dot{\rho}(t)$ given by (27) yields $\dot{\rho}(t) \geqslant 0$. Suppose $\rho(0) = 0$, then it is verified that $\rho(t) \geqslant 0$. Based on the definition of $\rho(t)$ given by (30), we get $qA_2/\eta - z(t) \geqslant 0$, namely,

$$z(t) \leqslant \frac{qA_2}{\eta}. \tag{34}$$

Up to now, we have proved that $g\dot{g} \leqslant -\rho_0|g(t)| + z(t)|g(t)|$ and $z(t) \leqslant qA_2/\eta$. Then, we consider two conditions in the following proof. □

Condition 1. $|g(t)| > g_0$

According to the definition of $z(t)$ shown in (28), we can get the first-order derivative of $z(t)$ as

$$\dot{z}(t) = -\dot{\rho}(t). \tag{35}$$

As per the definition of $\dot{\rho}(t)$ given by (27), it is known that $\dot{\rho}(t) = \omega|g(t)|$ under Condition 1. Hence,

$$\dot{z}(t) = -\omega|g(t)|. \tag{36}$$

Based on the Lyapunov function V defined in (31), we can obtain the first-order derivative of V as

$$\dot{V} = g\dot{g} + \frac{1}{\omega}z\dot{z}. \tag{37}$$

Substituting (36) into (37) yields

$$\dot{V} = g(t)\dot{g}(t) - z(t)|g(t)|. \tag{38}$$

Combining (33) with (38) we can conclude that

$$\dot{V} \leqslant -\rho_0|g(t)|. \tag{39}$$

Condition 2. $|g(t)| \leqslant g_0$

Under this condition, we get $\dot{\rho}(t) = 0$ according to (27). Based on the definition of $z(t)$ given by (28), we obtain

$$\dot{z}(t) = -\dot{\rho}(t) = 0. \tag{40}$$

Substituting (40) into (37) and combining (33) yields

$$\begin{aligned} \dot{V} &= g(t)\dot{g}(t) \\ &\leqslant -\rho_0|g(t)| + z(t)|g(t)|. \end{aligned} \tag{41}$$

From (41) we can evidently see that if $z(t) \leqslant 0$, then $\dot{V} \leqslant -\rho_0|g(t)|$. As expressed in (34), $z(t) \leqslant qA_2/\eta$ is always satisfied. Thus far, it is proved that outside the following rectangular region:

$$\Phi = \left\{(g,z) : |g| < g_0, 0 \leqslant z < \frac{qA_2}{\eta}\right\}, \tag{42}$$

the condition of $\dot{V} \leqslant -\rho_0|g(t)|$ is satisfied. Then, we construct an ellipse centered at the origin of Fig. 4 with the form of

$$\begin{aligned} \Omega &= \{(g,z) : V(g,z) < r\} \\ r &= \tfrac{1}{2}g_0^2 + \tfrac{1}{2\omega}\left(\tfrac{qA_2}{\eta}\right)^2 \end{aligned} \tag{43}$$

which encloses the rectangular region given by (42). Hence, if the parameter ξ can be chosen to satisfy

$$\frac{1}{4}\xi^2 > g_0^2 + \frac{1}{\omega}\left(\frac{qA_2}{\eta}\right)^2, \tag{44}$$

$g(t)$ will be forced to converge into the region of $|g(t)| < \xi/2$ in finite time.

Then, based on the definition of $g(t)$ given by (27), we obtain

$$\begin{aligned} |g(t)| &= \left|h(t) - \tfrac{1}{\eta}|\bar{\varphi}_{eq}(t)| - \xi\right| \\ &< \tfrac{1}{2}\xi. \end{aligned} \tag{45}$$

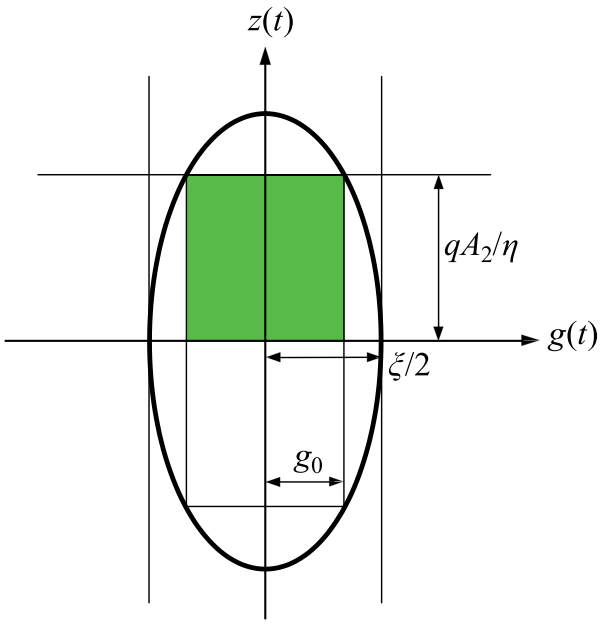

Fig. 4. Visualization of Ω and Φ.

Rearranging (45) yields

$$h(t) > \frac{1}{\eta}|\bar{\varphi}_{eq}(t)| + \frac{\xi}{2}. \tag{46}$$

Therefore, according to (29), the following inequality can be concluded:

$$h(t) > \frac{1}{\eta}|\bar{\varphi}_{eq}(t)| + \frac{\xi}{2} > |\varphi_{eq}(t)| = |\dot{A}(t)|. \tag{47}$$

The remaining proof follows the procedure in [33], which states that there exists a large enough $\mu > 0$ together with (47) such that the control law (19), (26) and (27) can achieve finite-time convergence property and the tracking error defined in (21) can be forced to converge to zero in finite time.

The proof is thus completed.

Remark 1. The stability of the overall control system has been verified in the sense of Lyapunov. However, the selection of control parameters is also of great importance for the practical implementation of the developed NASTSM controller in SbW systems since ideal tracking performance is usually compromised with the effect of unmodeled dynamics and measurement noises. Herein, we give the selection guideline of control parameters.

The parameter λ crucially determines the bandwidth of the sliding mode dynamics as shown in (22). A larger λ leads to a larger bandwidth indicating a faster response rate and higher tracking accuracy but at the cost of introducing more measurement noises. The parameter μ is known as the modulation gain associated with the discontinuous term in super-twisting sliding mode control [33]. The value of μ should be chosen sufficiently large to activate the sliding mode characteristics but not overlarge considering the discontinuity. The parameter ϵ affects the estimation rate of $\psi(t)$ as shown in (27), which should be given a small value for a fast estimation rate. From (27) we can also see that the parameter g_0 sets the threshold of the nested adaptive law to be activated. A smaller g_0 leads to smaller tracking errors compromised with measurement noises. The value of η is suggested to be in the range of $0 < \eta < 1$ according to [31]. The parameter ξ can be regarded as an offset of $g(t)$ as shown in (27). Overlarge value of ξ may cause system instability. Thus, the value of ξ is suggested to be set in the range of $1 < \xi < 2$ in our system. The parameters $\rho_0 > 0$ and $\omega > 0$ slightly affect the performance of the nested adaptive algorithm in our system. Thus, these two parameters can be tuned in reasonable ranges based on experimental performance.

3.2. Controller for comparison

In order to demonstrate the superiority of the developed NASTSM controller, a CASM controller proposed in [13] is employed to compare with the NASTSM controller. For simplicity, the control input of the CASM controller is straightly given:

$$\begin{aligned} u_{CASM} &= \tfrac{1}{b}\left[J_0\dot{E}\kappa + J_0\ddot{\delta}_r + c_0\dot{\delta} + f_0\mathrm{sign}(\dot{\delta}) + \varpi S + K\mathrm{sat}(S) + \hat{\rho}_\tau \tanh(\delta)\right] \\ K &= \bar{\Delta}_J|\dot{E}|\kappa + \bar{\Delta}_J|\ddot{\delta}_r| + \bar{\Delta}_c|\dot{\delta}| + \bar{\Delta}_f \\ \dot{\hat{\rho}}_\tau &= \left(\tfrac{i\varpi}{J_0} + is_l\right)\cdot S\cdot \tanh(\delta) \end{aligned} \tag{48}$$

where $\mathrm{sat}(*)$ is a saturation function with the boundary layer thickness of 0.8 [13]; $\tanh(*)$ is the hyperbolic tangent function defined in (16); E and S are the tracking error and the sliding variable under the CASM control defined as $E = \delta_r - \delta$, and $S = \dot{E} + \kappa E$, respectively; $\hat{\rho}_\tau$ is the estimation ρ_τ in the simplified self-aligning torque model given by (15); s_l is the Laplace operator; $\bar{\Delta}_J, \bar{\Delta}_c$ and $\bar{\Delta}_f$ are the upper bounds of the parametric uncertainties given by (6). Based on [13], the values of the control parameters are chosen as $\kappa = 15, \varpi = 45$ and $i = 2640$.

From the design of the NASTSM and CASM controllers, we can see that the difference between these two controllers is quite evident. The CASM controller relies on detailed information of a plant model to a large extent, especially the design of the adaptive estimation law is thoroughly based on the simplified model of self-aligning torques. On the contrary, the NASTSM controller requires less information of a plant model and can deal with the real time-varying self-aligning torque under various road conditions and vehicle velocities. In addition, the STSM control component in the NASTSM controller can produce a continuous control signal, which can alleviate the chattering that exists in the control input of the CASM controller to some extent.

4. Experimental results

Experiments are carried out on our SbW experimental platform shown in Fig. 1 to test the control performance of designed controllers. A fixed-step Euler solver with a sampling period of 0.001s is adopted for the experiment. To fairly and comprehensively compare the NASTSM controller with the CASM controller, three cases with different road paths,

various road conditions and time-varying vehicle velocities are arranged in experiments. In order to obtain a good balance between the tracking accuracy and the control robustness against system uncertainties, measurement noises and external disturbances, the values of the control parameters are selected as $\mu = 15, \rho_0 = 3.5, \eta = 0.9, \xi = 1.1, \lambda = 7, g_0 = 0.01, \omega = 25$ and $\epsilon = 0.01$.

4.1. Case 1: Slalom path

As a common path in reality, a slalom path is usually chosen to test the performance of a vehicle's steering system. In this case, we manipulate the steering wheel shown in Fig. 1(b) to generate an angle signal that is similar to a sinusoidal signal to mimic a slalom path for the vehicle to follow. Multiplying this angle measurement with a transmission gain from the steering wheel to the front wheels yields the reference command of the closed-loop control system. The values of front wheel cornering stiffness C_f and rear wheel cornering stiffness C_r are set as

$$\begin{cases} C_f = C_r = 12,000\ \text{N/rad}, & 0 < t \le 20\ \text{s}, \quad \text{snowy road} \\ C_f = C_r = 45,000\ \text{N/rad}, & 20 < t \le 40\ \text{s}, \quad \text{wet asphalt road} \\ C_f = C_r = 80,000\ \text{N/rad}, & 40 < t \le 60\ \text{s}, \quad \text{dry asphalt road} \end{cases} \tag{49}$$

to represent the condition of snowy, wet asphalt and dry asphalt road surfaces during the experiment, respectively. We also set a time-varying vehicle velocity V as

$$V = \begin{cases} 15 + 2t, & 0 < t \le 10\ \text{s} \\ 35 - 2(t-10), & 10 < t \le 20\ \text{s} \\ 15 + 2(t-20), & 20 < t \le 30\ \text{s} \\ 35 - 2(t-30), & 30 < t \le 40\ \text{s} \\ 15 + 2(t-40), & 40 < t \le 50\ \text{s} \\ 35 - 2(t-50), & 50 < t \le 60\ \text{s} \end{cases} \tag{50}$$

to represent the acceleration and deceleration motion of the vehicle. The experimental results of this case are shown in Fig. 5.

From Fig. 5 we can see that in this case, the control performance of the proposed NASTSM controller is superior to that of the CASM controller. The peak errors under the CASM control in three periods are 0.035 rad, 0.039 rad and 0.089 rad. However, the corresponding ones under the NASTSM control are 0.012 rad, 0.022 rad and 0.022 rad, which are much smaller. Besides, the steady-state errors under the CASM control are uneven compared with the ones under the NASTSM control. This is because that the CASM controller relies much on the simplified self-aligning torque model. When the vehicle velocity V is a constant, the simplified self-aligning torque model conforms to the real one well. However, if V is a time-varying one given by (50), the simplified self-aligning torque model cannot conform to the real one any more, which results in the deterioration of the tracking accuracy. On the contrary, the tracking errors under the NASTSM control are very even and remain in a small range of -0.025 rad to 0.025 rad due to the effect of the innovative nested adaptive law and the fast convergence rate of the STSM control component.

4.2. Case 2: Circular path

In this case, another common road path is considered, which is initially straight and then with a large circular curve. Likewise, we manipulate the steering wheel to generate a reference angle as if the vehicle is running along a circular road path. The duration of the experiment is set as 15 s. The front wheel cornering stiffness C_f and the rear wheel cornering stiffness C_r are set as $C_f = C_r = 45,000$ N/rad to represent a wet asphalt road condition. Furthermore, the vehicle velocity V is set as follows:

$$V = \begin{cases} 35, & 0 < t \le 2\ \text{s} \\ 35 - 2.5(t-2), & 2 < t \le 4\ \text{s} \\ 30, & 4 < t \le 9\ \text{s} \\ 30 - 2.5(t-9), & 9 < t \le 11\ \text{s} \\ 25, & 11 < t \le 15\ \text{s}. \end{cases} \tag{51}$$

The experimental results in this case are shown in Fig. 6.

As shown in Fig. 6, the tracking performance of the NASTSM controller is still superior to that of the CASM controller in this case. The peak error under the NASTSM control is 0.018 rad, which is much smaller than that under the CASM control (0.095 rad). During the whole experiment, the tracking errors of the NASTSM controller are forced to remain in a small region of -0.02 rad to 0.02 rad. However, from the beginning of steering front wheels (the 2nd second), it takes almost 4 s (the 2nd second to the 6th second) for the tracking error under the CASM control to converge to this region. This indicates that in the case of circular path following, the designed NASTSM controller still demonstrates higher tracking accuracy and stronger robustness against time-varying vehicle velocities compared with the CASM controller.

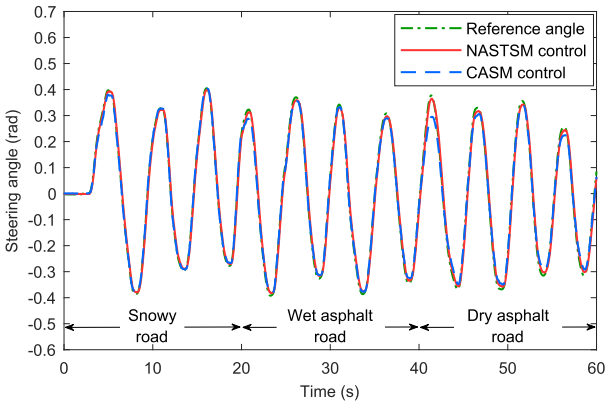

(a) Tracking profiles

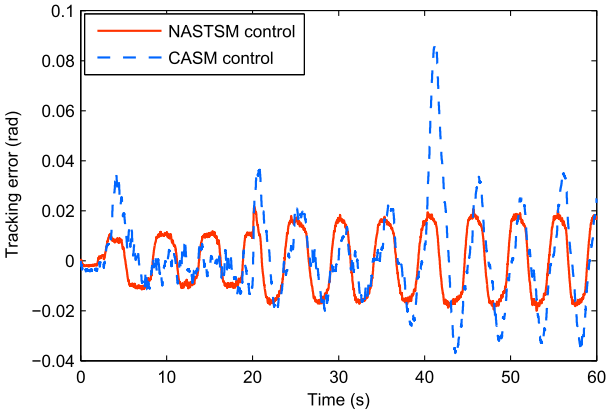

(b) Tracking errors

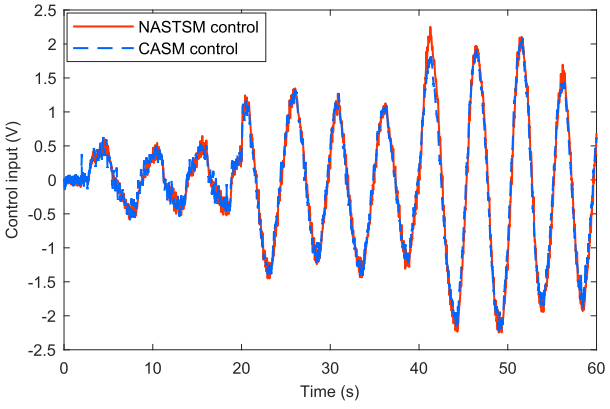

(c) Control inputs

Fig. 5. Control performance comparison in Case 1.

4.3. Case 3: Shock disturbance rejection

In reality, it is common for a running vehicle to come across small bumps, pot holes and road edges. When a rotating front wheel touches an obstacle, it may be forced to steer in a sudden resulting in an abrupt deviation of the vehicle from the original path, which may bring danger. Hence, whether the SbW system can reject the impact of shock disturbances and force the

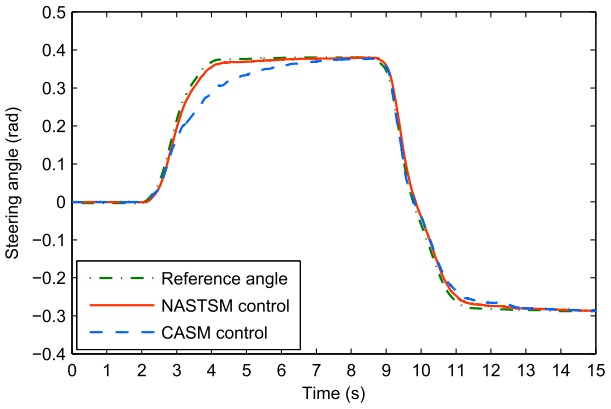

(a) Tracking profiles

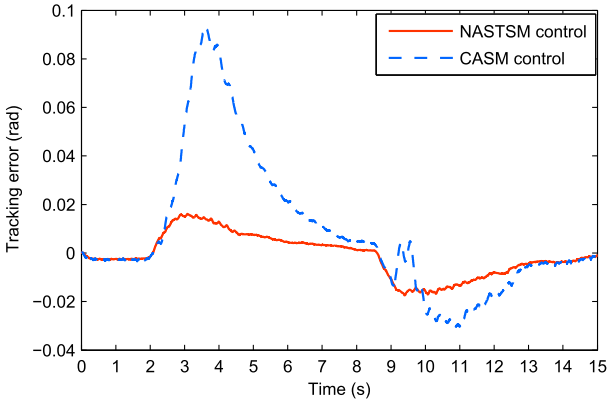

(b) Tracking errors

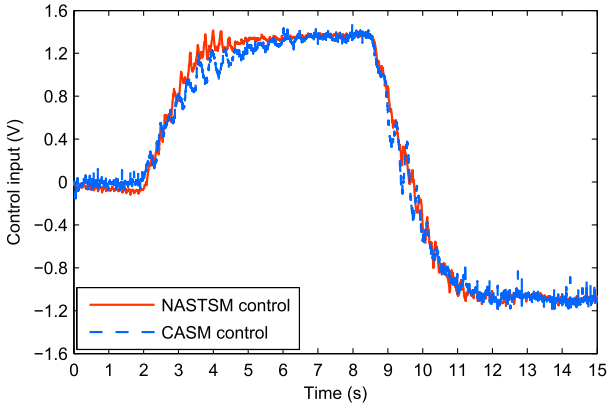

(c) Control inputs

Fig. 6. Control performance comparison in Case 2.

front wheels to steer back to the original position fast enough is of great importance. In this case, experiment with a duration of 10 s is carried out to test the convergence rate of the controllers. The reference signal is set as zero to mimic that the vehicle is running along a straight road path. Parameters C_f and C_r are set as $C_f = C_r = 45,000$ N/rad to represent a wet asphalt road condition. Besides, the vehicle velocity is set as a constant with the value of 35 m/s. The purpose of these settings is to exclude the interference of the change of road conditions and vehicle velocities. Referring to [34,35], a pulse voltage signal u_p

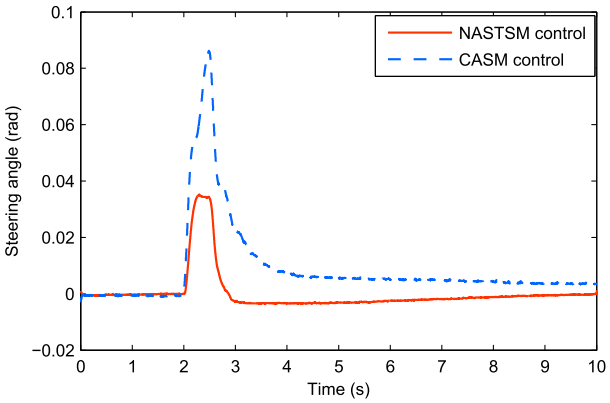

(a) Tracking profiles

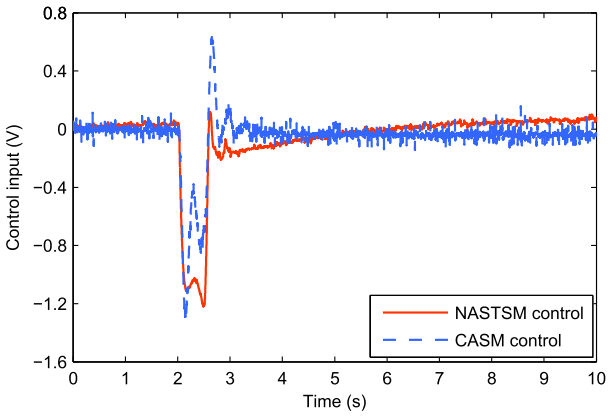

(b) Control inputs

Fig. 7. Control performance comparison in Case 3.

with an amplitude of 1.2 V and a width of 0.5 s is set as an input to the steering motor at the 2nd second to simulate the effect of the shock disturbance in experiments. This approach is similar to the generation of the effect of self-aligning torques as aforementioned. Thus, u_p is also independent from the control input u, and the effect generated by u_p can be treated as a shock disturbance of the whole system. The reason for the above setting is because of the constraints of our experimental platform. In the future work, we will generate real pulse torques to impose on the front wheels. The experimental results in this case are shown in Fig. 7.

As shown in Fig. 7, in this case, the peak error under the CASM control is 0.088 rad. However, the peak error under the NASTSM control is only 0.035 rad, which is evidently smaller. For the CASM control, it takes about 5 s (the 2nd second to the 7th second) for the tracking error to converge to a small region of -0.005 rad to 0.005 rad. In addition, at the end of the experiment, the tracking error only converges to 0.003 rad but not zero. However, for the NASTSM control, the time for the tracking error to converge into this region is only 1 s (the 2nd second to the 3rd second). Furthermore, the tracking error under the NASTSM control finally converges to zero at the end of the experiment. Hence, the superiority of the NASTSM controller in terms of higher tracking precision and faster convergence rate is also demonstrated in the case of shock disturbance rejection in comparison with the CASM controller.

5. Conclusion

In this paper, an NASTSM controller is designed for a vehicle SbW system. In the NASTSM control, an innovative nested adaptive law is proposed to handel the effect of complex time-varying external disturbances, and an STSM control component is adopted to generate smooth control signals while guaranteeing fast convergence property and strong control robustness. The stability of the NASTSM control system is verified in the sense of Lyapunov, and a CASM control scheme is proposed to compare with the NASTSM controller. Experiments are carried out for both the NASTSM and CASM controllers in three different cases under various road conditions and vehicle velocities. The experimental results of the NASTSM and CASM controllers are shown, compared and analyzed in detail. It is demonstrated that the developed NASTSM controller owns evident

superiority in terms of higher tracking accuracy, stronger robustness, faster convergence rate and most importantly, less dependence on the information of plant models compared with the CASM controller. Though the newly designed NASTSM controller requires a larger computational load for the control system hardware, the more and more sophisticated processor technology will definitely satisfy this requirement in actual implementation.

It should be noted that the self-aligning torque acting on the front wheels and the shock disturbance in Case 3 are not real ones but simulated in experiments. Thus, the experimental platform does not completely match the real scenario at this stage. However, our control design and experimental validation are still valuable for industrial references. Our future work is to improve the experimental platform as a real SbW-equipped vehicle which can run on the road. In addition, we will expand our research to more cutting-edge topics such as driverless vehicles based on the SbW technology.

References

[1] M.B.N. Shah, A.R. Husain, H. Aysan, S. Punnekkat, R. Dobrin, F.A. Bender, Error handling algorithm and probabilistic analysis under fault for CAN-based steer-by-wire system, IEEE Trans. Ind. Electron. 12 (3) (Jun. 2016) 1017–1034.
[2] H.E.B. Russell, J.C. Gerdes, Design of variable vehicle handling characteristics using four-wheel steer-by-wire, IEEE Trans. Control Syst. Technol. 24 (5) (Sep. 2016) 1529–1540.
[3] L. Yu, L. Ma, J. Song, X. Liu, Magnetorheological and wedge mechanism-based brake-by-wire system with self-energizing and self-powered capability by brake energy harvesting, IEEE/ASME Trans. Mechatronics 21 (5) (Oct. 2016) 2568–2580.
[4] L. Zhang, L. Yu, Z. Wang, L. Zuo, J. Song, All-wheel braking force allocation during a braking-in-turn maneuver for vehicles with the brake-by-wire system considering braking efficiency and stability, IEEE Trans. Veh. Technol. 65 (6) (Jun. 2016) 4752–4767.
[5] A. Beghi, L. Nardo, M. Stevanato, Observer-based discrete-time sliding mode throttle control for drive-by-wire operation of a racing motorcycle engine, IEEE Trans. Control Syst. Technol. 14 (4) (Jul. 2006) 767–775.
[6] M. Lindner, T. Tille, Design of highly integrated mechatronic gear selector levers for automotive shift-by-wire systems, IEEE/ASME Trans. Mechatronics 15 (6) (Dec. 2010) 961–968.
[7] T. Drage, J. Kalinowski, T. Braunl, Integration of drive-by-wire with navigation control for a driverless electric race car, IEEE Intell. Transp. Syst. Mag. 6 (4) (2014) 23–33.
[8] M. Bertoluzzo, G. Buja, R. Menis, Control schemes for steer-by-wire systems, IEEE Ind. Electron. Mag. 1 (1) (2007) 20–27.
[9] A. Balachandran, J.C. Gerdes, Design steering feel for steer-by-wire vehicles using objective measures, IEEE/ASME Trans. Mechatronics 20 (1) (Feb. 2015) 373–383.
[10] M.T. Do, Z. Man, C. Zhang, H. Wang, F.S. Tay, Robust sliding mode-based learning control for steer-by-wire systems in modern vehicles, IEEE Trans. Veh. Technol. 63 (2) (Feb. 2014) 580–590.
[11] P. Yih, J.C. Gerdes, Modification of vehicle handling characteristics via steer-by-wire, IEEE Trans. Control Syst. Technol. 13 (6) (Nov. 2005) 965–976.
[12] H. Wang, H. Kong, Z. Man, D.M. Tuan, Z. Cao, W. Shen, Sliding mode control for steer-by-wire systems with AC motors in road vehicles, IEEE Trans. Ind. Electron. 61 (3) (Mar. 2014) 1596–1611.
[13] Z. Sun, J. Zheng, Z. Man, H. Wang, Robust control of a vehicle steer-by-wire system using adaptive sliding mode, IEEE Trans. Ind. Electron. 63 (4) (Apr. 2016) 2251–2262.
[14] Z. Sun, J. Zheng, H. Wang, Z. Man, Adaptive fast non-singular terminal sliding mode control for a vehicle steer-by-wire system, IET Contr. Theory Appl. 11 (8) (Aug. 2016) 1245–1254.
[15] M. Mirzaei, H. Mirzaeinejad, Fuzzy scheduled optimal control of integrated vehicle braking and steering systems, IEEE/ASME Trans. Mechatronics 22 (5) (Oct. 2017) 2369–2379.
[16] F.-J. Lin, Y.-C. Hung, K.-C. Ruan, An intelligent second-order sliding-mode control for an electric power steering system using a wavelet fuzzy neural network, IEEE Trans. Fuzzy Syst. 22 (6) (Dec. 2014) 1598–1611.
[17] C. Huang, F. Naghdy, H. Du, Delta operator-based fault estimation and fault-tolerant model predictive control for steer-by-wire systems, IEEE Trans. Control Syst. Technol. 99 (2017) 1–8.
[18] J.E. Slotine, W. Li, Applied Nonlinear Control, Prentice-Hall, Englewood Cliffs, NJ, USA, 1991.
[19] R. Gupta, A. Ghosh, A. Joshi, Multiband hysteresis modulation and switching characterization for sliding-mode-controlled cascaded multilevel inverter, IEEE Trans. Ind. Electron. 57 (7) (Jul. 2010) 2344–2353.
[20] F.-J. Lin, J.-C. Hwang, P.-H. Chou, Y.-C. Hung, FPGA-based intelligent-complementary sliding-mode control for PMLSM servo-drive system, IEEE Trans. Power Electron. 25 (10) (Oct. 2010) 2573–2587.
[21] S.-Y. Chen, S.-S. Gong, Speed tracking control of pneumatic motor servo systems using observation-based adaptive dynamic sliding-mode control, Mech. Syst. Sig. Process. 94 (15) (2017) 111–128.
[22] X. Li, Y. Wang, Sliding-mode control combined with improved adaptive feedforward for wafer scanner, Mech. Syst. Sig. Process. 103 (15) (Mar. 2018) 105–116.
[23] Z. Man, X. Yu, Terminal sliding mode control of MIMO systems, IEEE Trans. Circuits Syst. I 44 (11) (Nov. 1997) 1065–1070.
[24] Y. Feng, X. Yu, Z. Man, Non-singular terminal sliding mode control of rigid manipulators, Automatica 38 (12) (Dec. 2002) 2159–2167.
[25] T. Gonzalez, J.A. Moreno, L. Fridman, Variable gain super-twisting sliding mode control, IEEE Trans. Autom. Control 57 (8) (Aug. 2012) 2100–2105.
[26] C. Kunusch, P.F. Puleston, M.A. Mayosky, J. Riera, Sliding mode strategy for PEM fuel cells stacks breathing control using a super-twisting algorithm, IEEE Trans. Control Syst. Technol. 17 (1) (Jan. 2009) 167–174.
[27] N. Ahmadian, A. Khosravi, P. Sarhadi, Adaptive control of a jet turboshaft engine driving a variable pitch propeller using multiple models, Mech. Syst. Sig. Process. 92 (2017) 1–12.
[28] Y. Wu, G. Li, Adaptive disturbance compensation finite control set optimal control for PMSM systems based on sliding mode extended state observer, Mech. Syst. Sig. Process. 98 (1) (Jan. 2018) 402–414.
[29] A. Ayadi, M. Smaoui, S. Aloui, S. Hajji, M. Farza, Adaptive sliding mode control with moving surface: experimental validation for electropneumatic system, Mech. Syst. Sig. Process. 109 (1) (Sep. 2018) 27–44.
[30] Y. Hu, W. Gu, H. Zhang and H. Chen, Adaptive robust triple-step control for compensating cogging torque and model uncertainty in a DC motor, IEEE Trans. Syst., Man, Cybern., Syst., availabe online.
[31] C. Edwards, Y.B. Shtessel, Adaptive continuous higher order sliding mode control, Automatica 65 (Mar. 2016) 183–190.
[32] Y. Yamaguchi, T. Murakami, Adaptive control for virtual steering characteristics on electric vehicle using steer-by-wire system, IEEE Trans. Ind. Electron. 56 (5) (May 2009) 1585–1594.
[33] V.I. Utkin, A.S. Poznyak, Adaptive sliding mode control with application to super-twist algorithm: equivalent control method, Automatica 49 (Oct. 2012) 39–47.
[34] D.Q. Truong, K.K. Ahn, Force control for hydraulic load simulator using self-tuning grey predictor-fuzzy PID, Mechatronics 19 (2) (Mar. 2009) 233–246.
[35] J. Zheng, M. Fu, Y. Wang, C. Du, Nonlinear tracking control for a hard disk drive dual-stage actuator system, IEEE/ASME Trans. Mechatronics 13 (5) (Oct. 2008) 510–518.